2B.3 ASSESSING ATMOSPHERIC STABILITY AND THE IMPACTS ON WIND CHARACTERISTICS AT AN ONSHORE WIND FARM

Sonia Wharton*[,1] and Julie Lundquist[2]

[1] Atmospheric, Earth and Energy Division, Lawrence Livermore National Laboratory, Livermore, California
[2] Dept. Atmospheric and Ocean Sciences, University of Colorado at Boulder

1. ABSTRACT

As the average hub height and blade diameter of new wind turbine installations continues to increase, turbines typically encounter higher wind speeds, which enable them to extract large amounts of energy, but they also face challenges due to the complex nature of wind flow and turbulence in the planetary boundary layer (PBL). Wind speed, direction and turbulence vary across a turbines' rotor disk, in part on whether the PBL is stable, neutral or convective. To assess the influence of stability on wind characteristics, we utilized a unique dataset including meteorological tower observations, surface flux observations, and high resolution measurements of wind speed and turbulence from a remote-sensing Sound Detection and Ranging (SODAR) instrument. We compared several approaches to defining atmospheric stability to the Obukhov length (*L*). Typical wind farm observations enable the calculation only of a wind shear exponent (α) or horizontal turbulence intensity (I_U) from cup anemometers, while SODAR gives measurements of turbulence intensity (I) in the latitudinal (I_u), longitudinal (I_v) and vertical (I_w) directions and turbulence kinetic energy (*TKE*) at multiple heights in the rotor disk. Two methods for calculating I_U from SODAR data are presented here. The derived SODAR stability parameters were in high agreement with the more physically-robust *L*, with *TKE* exhibiting the best agreement, and show promise for accurate characterizations of stability at an onshore wind farm. Vertical profiles of wind speed and turbulence, which are likely to affect turbine power performance, were highly correlated to the predicted stability regimes.

2. INTRODUCTION AND METHODS

2.1 *Site Description*

This study was conducted at a wind farm in western North America at an elevation of near-sea level with some marine boundary layer influences. The area experiences strong land-sea temperature differences, particularly during the summer months when the land is much warmer than the coastal Pacific waters. The resulting pressure gradient produces strong onshore flow consistently from the westerly or southwesterly direction. The site has two distinct seasons: a wet, cool winter with frequent synoptic storms and a dry, warm summer with very little convective storm activity. The landscape both upwind of and at the wind farm is grassland on rolling hills of mildly complex terrain. A number of horizontal-axis, three-bladed turbines with a rotor diameter of ~80 m were in operation at the wind farm. The blades interact with the instantaneous wind speed within a disk-shaped area across heights of 40 m to 120 m above ground level (AGL), where 40 m is the minimum blade tip height and 120 m is the maximum blade tip height. The nacelle and power generator are located at 80 m AGL (referred to as hub-height).

The wind farm has two meteorological towers with vertical arrays of cup anemometers (#40, NRG Systems, Hinesburg, VT, USA) from 30-80 m. A SODAR (Model4000, Atmospheric Systems Corporation, Santa Clarita, CA, USA) collected high resolution, three-axis wind velocity data. SODAR enabled calculation of a wind shear exponent, latitudinal, longitudinal and vertical turbulence intensities, and turbulence kinetic energy at 10 m intervals from 20 to 200 m AGL. In addition, the Obukhov length was obtained from three-axis wind velocity and surface heat flux measurements (WindMaster Pro 3-axis ultrasonic anemometer, Gill Instruments Ltd, Hampshire, England) from a flux station approximately 15 km away in similar terrain. All meteorological measurements except for the Obukhov length were averaged over a 10-minute period following standards found in IEC (2005). Measurements of wind speed, momentum flux and heat flux used in the Obukhov length were available as 30-minute averages.

2.2 *Stability Parameter Calculations*

Stability classification schemes for the planetary boundary layer (PBL) are typically based on vertical profiles of potential temperature θ (called the lapse rate, $\frac{d\theta}{dz}$), the gradient Richardson number *Ri* (the ratio of thermally produced/consumed turbulence to mechanically produced/dissipated turbulence) (e.g., Kaimal and Finnigan 1994), or the Obukhov length *L* (a scaling parameter used to indicate atmospheric mixing conditions in the surface layer) (e.g., Mahrt 1999). Vertical profiles of potential temperature give the most straightforward indication of whether the boundary layer is statically stable ($\frac{d\theta}{dz} > 0$), statically unstable ($\frac{d\theta}{dz} < 0$) or neutral ($\frac{d\theta}{dz} = 0$), although a complete temperature profile requires either multiple instruments on a very tall

* *Corresponding author address*: Sonia Wharton, Atmospheric, Earth and Energy Division, L-103, PO Box 808, Lawrence Livermore National Laboratory, Livermore, CA 94551. Email: wharton4@llnl.gov
Webpage: https://energy.llnl.gov/

meteorological tower or a remote sensing platform equipped with a temperature profiler. Because these can be very expensive, boundary-layer studies often instead rely on the Obukhov length to characterize stability, which requires a sonic anemometer above the canopy, but this approach may not be the most ideal for wind energy applications because *L* does not account for top-down forced boundary layers such as those that occur at night during low-level jets (Mahrt and Vickers 2002). Therefore, a more universal, yet accurate stability parameter is needed in the wind industry, based on available instrumentation.

Wind farms have conventionally inferred local stability either from a wind shear exponent α, estimated from cup anemometers at two measurement heights or turbulence intensity *I*, often from a single cup anemometer near hub height. High magnitudes of wind shear suggest a stable boundary layer whereby the turbine blades are likely to encounter strongly stratified flow across the rotor disk (e.g., much higher wind speeds at the top of the rotor than at the bottom) which, if very intense, may cause out-of-plane bending loads on the blades and damage turbine components. Low values of wind shear indicate convective or well-mixed conditions across the rotor and a more uniform velocity profile. SODAR and cup anemometer wind velocities were used to calculate α using the power law expression (Elliott et al. 1987), in Eq (1),

$$U(z) = U_R\left(\frac{z}{z_R}\right)^{\alpha} \quad (1)$$

where *U* is the mean horizontal wind speed (m s^{-1}) at height *z* (m) and U_R is the mean horizontal wind speed (m s^{-1}) at a reference height z_R (m); by convention height z_R is closer to the ground than *z*. The wind shear exponent is traditionally used to estimate variations in available wind power with height when direct measurements of wind speed across the rotor are unavailable. Here, three wind shear exponents were calculated using SODAR wind speed measurements at 40, 80 and 120 m: α_{40_120} parameterizes stability across the entire rotor disk, α_{40_80} parameterizes stability across the lower half of the rotor disk, and α_{80_120} parameterizes stability across the upper half. A fourth α, α_{50_80}, was calculated using the 50 and 80 m cup anemometer data for comparison to SODAR. The wind shear exponent describes the degree of atmospheric stability based on the presence (shear or no shear) and amount (low or high shear) of stratified flow but is not a direct measure of stability.

Turbulence intensity *I* (%) uses measurements of velocity fluctuations in the boundary layer to characterize stability and is a statistical descriptor of the overall level of turbulence in relation to mean wind speed. High *I* magnitudes indicate that a significant portion of the wind is composed of turbulent flow while low *I* values indicate laminar flow with less turbulence. Three-component turbulence intensities can be calculated when *u*, *v*, and *w* observations are available, as from a SODAR or sonic anemometer. These include I_u, the latitudinal turbulence intensity, I_v, the longitudinal turbulence intensity, and I_w, the vertical turbulence intensity. The first turbulence intensity I_u describes the relative amount of turbulence in the x direction in relation to the mean horizontal wind speed, following Shaw et al. (1974),

$$I_u = \frac{\sigma_u}{U} \quad (2)$$

where σ_u (m s^{-1}) is standard deviation of the latitudinal velocities over a 10-minute period. Likewise turbulence intensity in the longitudinal direction is,

$$I_v = \frac{\sigma_v}{U} \quad (3)$$

and turbulence intensity in the vertical direction is,

$$I_w = \frac{\sigma_w}{U} \quad (4)$$

Note that calculations of a longitudinal I_v or vertical I_w are not possible with a cup anemometer since the instrument measures only horizontal wind speed (*U*), and not the velocity components *u*, *v* and *w*. We assume here that the cup anemometer is insensitive to any changes in the vertical velocity. Using a cup anemometer, turbulence intensity is determined by calculating a horizontal turbulence intensity as in Eq (5),

$$I_{Ucup} = \frac{\sigma_U}{U} \quad (5)$$

SODAR *I* magnitudes are not directly comparable to those from the cup anemometer because the expressions for *I* in Eqs (2-4) are not equal to *I* in Eq (5). In order to directly compare the instruments, we calculated two alternative expressions for horizontal turbulence intensity from the SODAR which include the standard deviations of *u* and *v*. Eq (6) appears to be the standard way to calculate SODAR I_U in the wind energy industry, whereby I_U is the average of the latitudinal and longitudinal turbulence fluctuations and assumes that turbulence is isotropic,

$$I_{U1SODAR} = \frac{0.5(\sigma_u + \sigma_v)}{U} \quad (6)$$

We follow methodology adopted by micrometeorologists in Eq (7) and calculate a horizontal turbulence intensity based on the square-root of the sum of turbulence in the latitudinal and longitudinal velocities,

$$I_{U2SODAR} = \frac{\sqrt{(\sigma_u^2 + \sigma_v^2)}}{U} \quad (7)$$

The expression for turbulence intensity in Eq (7) is found in Chan (2008) and is similar to derivations found in Shaw et al. (1974) and Weber (1998). Note that Eq (6) (the "averaging method") and Eq (7) (the "square-root method) will not give identical magnitudes of I_U even if the turbulence is isotropic because the two expressions for horizontal turbulence are not equal.

Related to SODAR *I*, turbulence kinetic energy *TKE* (m^2 s^{-2}) was calculated from SODAR data using the three turbulence components as in Eq (8),

$$TKE = \frac{1}{2}(\sigma_u^2 + \sigma_v^2 + \sigma_w^2) \quad (8)$$

TKE is a measure of the intensity of turbulence and is directly related to the transport of momentum (shear-generated turbulence that is strongest in the horizontal direction) and heat (thermal-generated turbulence in the vertical direction) through the boundary layer. Hence, *TKE* is the sum of all measurable sources of turbulence, both convective and mechanically-generated.

Finally, a nearby flux station provided 3-axis wind velocity and surface heat flux data from a sonic anemometer and fast-response thermocouple from which the stability length scale *L* (Obukhov length) was calculated. *L* (m) is used as a scaling parameter to indicate atmospheric mixing conditions in the surface layer, following Monin-Obukhov similarity theory (Monin and Obukhov 1954, Obukhov 1971, Nieuwstadt 1984, Stull 1988), and is calculated using Eq (9),

$$L = -\frac{\theta_v \cdot u_*^3}{k \cdot g \cdot \overline{w'\theta_v'}} \quad (9)$$

where θ_v is virtual potential temperature (K), *k* is the von Karman constant (0.4), *g* is acceleration due to gravity (9.8 m s^{-2}), $\overline{w'\theta_v'}$ is surface heat flux (W m^{-2}), and friction velocity u_* (m s^{-1}) is defined from the turbulence momentum fluxes, $u_* = (\overline{u'v'}^2 + \overline{v'w'}^2)^{1/4}$.

2.3 *Stability Classifications*

For each 10 minute period we described the boundary layer stability conditions based on the Obukhov length *L*, wind shear exponent α (at various heights in the rotor disk), turbulence intensity *I* (at 80 m AGL), and turbulence kinetic energy *TKE* (at 80 m AGL), and classified the time period as belonging to one of five stability classes: strongly stable, stable, neutral (includes slightly stable and slightly convective), convective, or strongly convective. Descriptions of the stability regimes are given in Table 1. The stability thresholds are listed in Table 2 and are based largely on published values, although the criteria have been slightly modified according to the range of atmospheric conditions and terrain observed at this wind farm.

Boundary Layer Properties
Very Stable: highest wind shear in rotor disk, low turbulence unless a low-level jet is present which can produce strong turbulence at the top of the rotor.
Stable: moderate to high wind shear in rotor disk, low turbulence.
Neutral: generally strongest wind speeds throughout the rotor disk. Wind speed increases logarithmically with height. Moderate turbulence.
Convective: lower wind speeds, low wind shear in the rotor disk, moderate to high turbulence.
Very Convective: lowest wind speeds, very little wind shear in the rotor disk, highly turbulent due to large. buoyant eddies.

Table 1. General PBL conditions according to stability regime.

Stability class	***L***	**α**	**I_{Ucup} & $I_{U1SODAR}$**	**$I_{U2SODAR}$**	***TKE***
strongly stable	0 < L < 100	α > 0.3	I_U < 5%	I_U < 8%	*TKE* < 0.4
stable	100 < L < 600	0.2 < α < 0.3	5 < I_U < 8%	8 < I_U < 10%	0.4 < *TKE* < 0.7
neutral	|L| > 600	0.1 < α < 0.2	8 < I_U < 11%	10 < I_U < 13%	0.7 < *TKE* < 1.0
convective	- 600 < L < - 50	0.0 < α <0.1	11 < I_U < 14%	13 < I_U < 20%	1.0 < *TKE* < 1.4
strongly convective	-50 < L < 0	α < 0.0	I_U > 14%	I_U > 20%	*TKE* > 1.4

Table 2. Classification thresholds for each stability parameter. Note that neutral conditions include weakly stable and weakly convective regimes. *I* (%) and *TKE* (m^2 s^{-2}) thresholds are at hub-height (80 m); α (dimensionless) is across the rotor disk (40 to 120 m).

3. RESULTS AND DISCUSSION

3.1 *Stability Parameter Analysis*

The percentage of summertime periods defined as stable (includes moderate and strong), neutral (includes weakly stable and weakly convective) and convective (includes moderate and strong) by the Obukhov length, wind shear exponent (across 40 to 120 m), horizontal turbulence intensity (at 80 m), and turbulence kinetic energy (at 80 m) are shown in Figure 1.

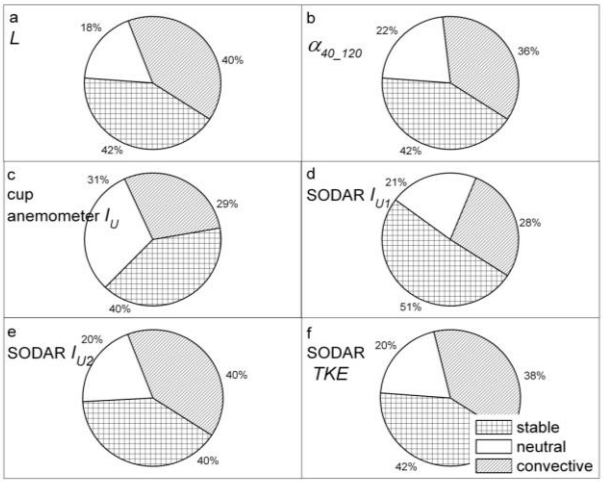

Figure 1. Percentage of 10-minute periods classified as stable, neutral or convective according to the stability parameters. The stability parameters with highest agreement to *L* are *TKE* and SODAR I_{U2}.

The Obukhov length indicated stable: neutral: convective conditions in a 42:18:40 ratio with weakly stable and weakly convective regimes included in the neutral category (Figure 1a). As expected, daytime

periods were primarily classified as strongly convective, convective, or weakly convective, while nighttime periods were strongly stable, stable, or slightly stable. Stable conditions were present on nearly every nighttime hour during the spring and summer months. The stability parameters, α_{40_120} (1b), $I_{U2SODAR}$ (1e) and *TKE* (1f) showed highest agreement with *L* and predicted stable: neutral: convective ratios of 42:22:36, 40:20:40, and 42:20:38, respectively, while I_{Ucup} (1c) and $I_{U1SODAR}$ (1d) underpredicted convective conditions by more than 10%.

Mean diurnal patterns for all stability parameters during the spring and summer period are shown in Figure 2 and further indicate average convective atmospheric conditions during the day and stable conditions at night. The normalized Obukhov length is shown in Figure 2a for comparison to the derived stability parameters. Figure 2b shows three SODAR wind shear exponents α_{40_120} (wind shear across the entire rotor disk), α_{40_80} (shear across the lower half), and α_{80_120} (shear across the upper half) in comparison to the meteorological tower α_{50_80}. Diurnal wind shear variability was large and all four wind shear exponents were, on average, greater than 0.2 at night (indicating high shear and stable conditions) and less than 0.1 during the day (indicating low shear and convective conditions). During the day, wind shear was generally higher in the lower half of the rotor disk than the upper half. Magnitudes of SODAR α_{40_80} and cup anemometer α_{50_80} were very similar as expected although the cup anemometer indicated slightly less wind shear during the daylight hours.

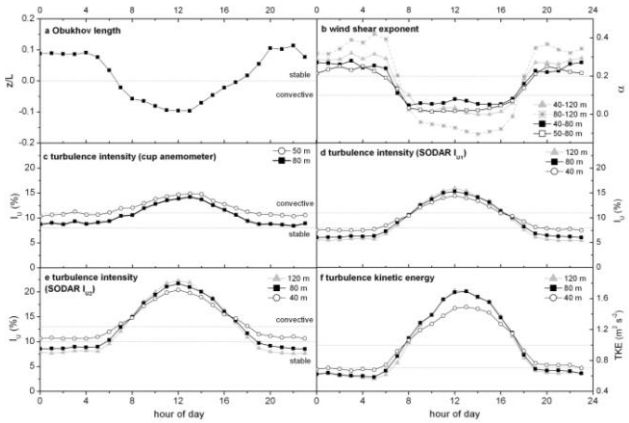

Figure 2. Mean diurnal plots of stability parameters show convective conditions during the day and stable conditions at night in agreement with *z/L* while α_{120_40}, $I_{U2SODAR}$, and *TKE* show the highest amount of diurnal variability. The dotted lines represent stable and convective thresholds for each stability parameter as listed in Table 2.

Diurnal magnitudes of I_U indicated systematic differences between the cup anemometer and SODAR as well as differences in the methodology used to calculate SODAR horizontal turbulence. I_{Ucup} indicated on average higher turbulence intensities closer to the ground (50 m versus 80 m) during both nighttime and daytime hours (Figure 2c). Mean cup anemometer I_U was 13.5% at 50 m and 12.7% at 80 m during the midday hours and 9.7% at 50 m and 7.9% at 80 m at night. The first SODAR-derived horizontal turbulence intensity $I_{U1SODAR}$ showed a similar amount of diurnal variability as I_{Ucup} although the SODAR parameter showed highest daytime *I* magnitudes at 120 m and highest nighttime *I* values closer to the ground at 40 m. Mean nighttime 40 m (80 m) (120 m) $I_{U1SODAR}$ was 7.6% (6.2%) (5.5%). Mean daytime 40 m (80 m) (120 m) $I_{U1SODAR}$ was 13.5% (14.4%) (14.8%). These differences in $I_{U1SODAR}$ with height and time of day are realistic given that turbulence at night is shear-driven (e.g., friction along the surface) while daytime turbulence is dominated by large, buoyant eddies.

The second SODAR-derived *I* parameter, $I_{U2SODAR}$, showed a greater amount of diurnal variability than seen either with I_{Ucup} or $I_{U1SODAR}$ and is shown in Figure 2e. Hub-height $I_{U2SODAR}$ ranged from 20.3% during midday to 8.6% at night. $I_{U2SODAR}$ also showed slightly more stratification in *I* with height during the nighttime hours: mean *I* =10.8% at 40 m and 7.7% at 120 m. The largest differences between hub-height I_{Ucup}, $I_{U1SODAR}$ and $I_{U2SODAR}$ magnitudes occurred during the midday hours and peak values ranged from 14.2% (I_{Ucup}) to 21.7% ($I_{U2SODAR}$). The cup anemometers systematically measured smaller turbulence intensities during the daytime hours as compared to the SODAR. Further analysis showed that the instrument differences came largely from differences in the 10-minute standard deviations (σ_U). Cup anemometer σ_U magnitudes were generally lower than both methods used to calculate SODAR σ_U. The "square-root" method (Equation 7) yielded up to 5% higher I_U magnitudes during the day than did the "averaging method" (Equation 6). This greater range of *I* magnitudes made it possible to distinguish very convective conditions from moderately convective using $I_{U2SODAR}$.

The mean diurnal pattern for turbulence kinetic energy at heights of 40, 80 and 120 m appears in Figure 2f. The amount of diurnal variability in *TKE* was very similar to that observed for $I_{U2SODAR}$, indicating the utility of $I_{U2SODAR}$ to segregate the data into detailed stability classes. As with the SODAR *I* parameters, nighttime *TKE* decreased with height, while daytime *TKE* increased with height. Mean daytime (nighttime) *TKE* magnitudes were 1.60 m^2 s^{-2} (0.63 m^2 s^{-2}) at 120 m, 1.58 m^2 s^{-2} (0.64 m^2 s^{-2}) at 80 m, and 1.42 m^2 s^{-2} (0.71 m^2 s^{-2}) at 40 m. As expected, nighttime *TKE* magnitudes were indicative of stable, stratified flows while daytime *TKE* showed a much more energetic atmosphere.

3.2 *Stability Influence on Wind Velocity and Turbulence Profiles*

The following analyses use $I_{U2SODAR}$ (at hub-height) to quantify the effects of stability regime on the rotor disk wind speed and turbulence profiles during spring and summer. Stability-correlated variability was very high during the spring and summer months. 10-minute wind speeds at 40, 80 and 120 m were averaged by stability class in Figure 3. Maximum wind speeds were observed during stable conditions, at all heights, with

the largest stability-related differences occurring at the top of the rotor during the summer months. For example, in the summer, mean 120 m wind speed was 14.0 m s^{-1} during very stable conditions in comparison to 3.0 m s^{-1} during very convective conditions (Figure 3b). Hub height wind speed was also significantly lower ($P < 0.05$) during convective or strongly convective conditions than during stable or neutral regimes. As expected, convective conditions showed almost no wind speed variability with height while wind speeds were highly stratified across the rotor during stable and very stable conditions.

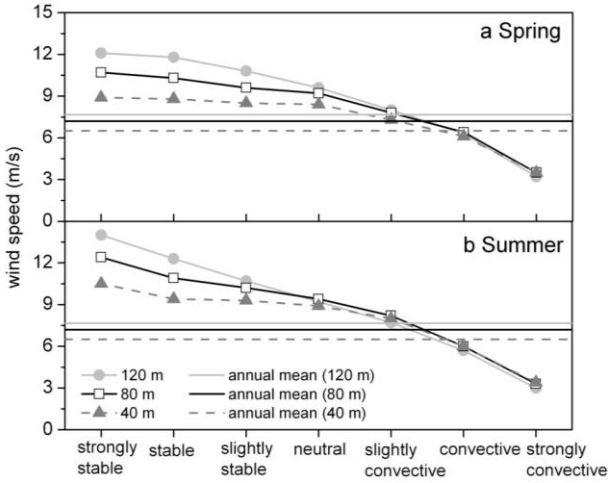

Figure 3. Mean wind speed across the turbine rotor (40, 80, and 120 m) according to stability class. The largest stability influences occurred during the summer season when strongly stable and strongly convective wind speeds differ by more than 10 m s^{-1}. The horizontal lines show the annual mean wind speed at each height.

The complete vertical profiles (20 m to 160 m) of wind speed and *TKE* from SODAR are shown in Figure 4, segregated according to stability class. The figure shows clear distinctions in how wind speed varies with height depending on atmospheric stability. Additionally, it is clear that a constant wind shear exponent is not sufficient in predicting the mean wind speed profile under non-neutral conditions. Using wind speed observations at 80m and assuming an α = 1/7 in equation (1), an extrapolated mean wind profile may be calculated. Significant differences between measured *U* and this extrapolated *U* occurred during both stable and convective conditions in the warm season. As a general rule, wind speed increased faster with height than the power law predicted during stable conditions. Conversely, wind speed was nearly constant or decreased slightly with height during convective conditions.

During strongly stable conditions, wind speed at the top of the rotor approached 14 m s^{-1} and was 1.5 m s^{-1} greater than the predicted wind speed at this height (using α = 1/7), while in the lower half of the rotor, *U* was 10 m s^{-1}, a full meter per second slower than predicted with the power law (Figure 4a). In contrast, during convective conditions, wind speed was overestimated in the top half of the rotor by 1.5 to 2.0 m s^{-1}, and underestimated in the lower half by 0.5 m s^{-1} by the power law. The vertical *U* profile during near-neutral or weakly stable conditions was well predicted by α = 1/7. *TKE* decreased slightly with height (up to 100 m) during very stable conditions, was nearly constant with height during near-neutral conditions, and increased rapidly with height during strongly convective conditions (Figure 4b). The largest changes in *TKE* with height were observed in the lower half of the rotor, regardless of stability regime. A slight peak in *TKE* is visible during very stable conditions at 140 m, which may indicate the presence of low-level jets since a wind maxima is also present at 150 m, although confirmation of LLJs is not possible without further investigation.

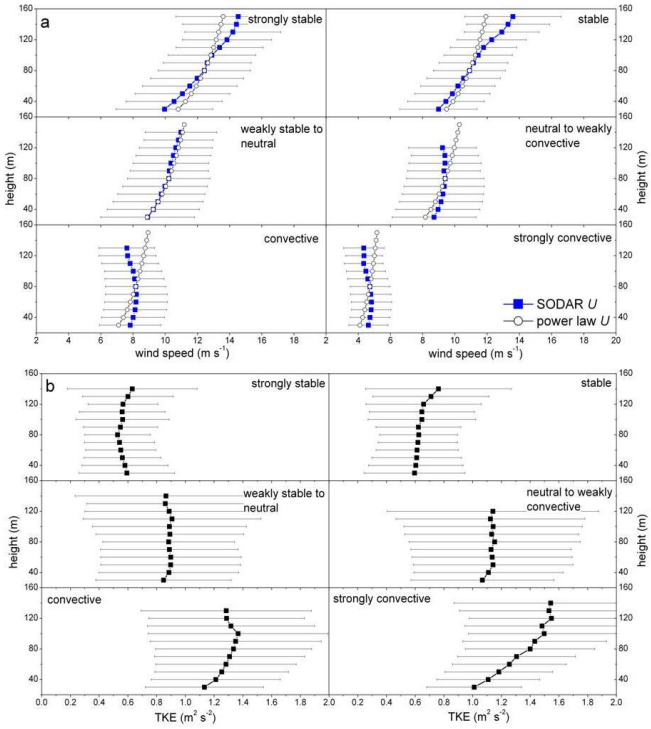

Figure 4. Summer vertical profiles (20 m to 160 m) of SODAR (a) mean wind speed and (b) turbulence kinetic energy during strongly stable, stable, near-neutral, convective, and strongly convective conditions. For reference, the turbine rotor disk covers heights of 40 to 120 m. Missing data points are due to poor data recovery. The error bars are ± one standard deviation from the mean. Also plotted in 4a is the predicted wind speed profile (open circles) based on the 1/7th power law (α = 0.14) and 80 m wind speed.

4. CONCLUSIONS

Our observation that wind speed and turbulence kinetic energy vary with height in a predictable way depending on atmospheric stability highlights some of the numerous advantages of deploying more sophisticated meteorological instruments at large wind farms instead of relying on cup anemometers for sparse measurements of wind speed and turbulence intensity at hub-height and possibly at one or more heights in the

rotor disk. The high-resolution SODAR data confirmed that a constant wind shear exponent as assumed by the power law leads to grossly inaccurate predictions of wind speeds at the top and bottom of the rotor disk, particularly during strongly stable and strongly convective conditions. These inaccuracies can be either over-assessments of the wind resource (as seen in the turbulent time periods at this site) or under-assessments of the wind resource (as seen in the stable time periods at this site) and are consistent with findings in Sisterson et al. (1983). Considering that the accuracy of wind speed across the entire rotor disk is critical to wind energy applications, we recommend that wind farms invest in more sophisticated meteorological instrumentation such as remote sensing platforms which give high spatial resolution velocity measurements. Furthermore, our results strongly suggest that on-site, near-real-time estimates of stability would enable a wind farm to more accurately predict the available wind resource.

5. ACKNOWLEDGEMENTS

The authors express great appreciation to Iberdrola Renewables, Inc., for the collection, provision, and insightful discussion of this rich dataset, and in particular, thank Dr. Justin Sharp, Dr. Mike Zulauf, and Jerry Crescenti. We also acknowledge Dr. Dennis Baldocchi and Dr. Matteo Detto for their contribution of the off-site, sonic anemometer data. This work was funded by the Department of Energy's Wind and Water Power Program Office under the Renewable Systems Interconnect Support program (BNR Code EB2502010) managed by Stan Calvert. LLNL is operated by Lawrence Livermore National Security, LLC, for the DOE, National Nuclear Security Administration under Contract DE-AC52-07NA27344. LLNL-PROC-443731

6. REFERENCES

Chan, P.W., 2008: Measurement of turbulence intensity profile by a mini-sodar. *Meteorol. Appl.*, 15, 249-258.

Elliott, D.L., Holliday, C., Barchet, W., Foote, H., Sandusky, W., 1987: *Wind Energy Resource Atlas of the United States*. DOE/CH 10093-4, Golden, Colorado: Solar Energy Research Institute, 210 pp.

International Electromechanical Commission (IEC), 2005: *Wind Turbines - Part 12-1: Power performance measurements of electricity producing wind turbines*. Technical Report No, IEC 61400-12-1.

Kaimal, J.C., Finnigan, J.J., 1994: *Atmospheric Boundary Layer Flows – Their Structure and Measurement*. Oxford University Press: New York, 287 pp.

Mahrt, L., 1999: Stratified atmospheric boundary layers. *Boundary-layer Meteorol.*, 90, 375-396.

Mahrt, L., Vickers D., 2002: Contrasting vertical structures of nocturnal boundary layers. *Boundary-layer Meteorol.*, 105, 351-363.

Monin, A.S., Obukhov, A.M., 1954: Basic laws of turbulent mixing in the ground layer of the atmosphere. *Trans. Geophys. Inst.*, 151, 163-187.

Nieuwstadt, F.T.M., 1984: The turbulent structure of the stable, nocturnal boundary layer. *J. Atmos. Sci.*, 41, 2202-2216.

Obukhov, A.M., 1971: Turbulence in an atmosphere with a non-uniform temperature. *Boundary-layer Meteorol.,* 2, 7-29.

Shaw, R.H., Hartog, G.D., King, K.M., Thurtell, G.W., 1974: Measurements of mean wind flow and three-dimensional turbulence intensity within a mature corn canopy. *Agric. Meteorol.,* 13, 419-425.

Sisterson, D.L., Hick, B.B., Coulter, R.L., Wesely, M.L., 1983: Difficulties in using power laws for wind energy assessment. *Solar Energy*, 31, 201-204.

Stull, R.B., 1988: *An Introduction to Boundary Layer Meteorology*. Kluwer Academic Publishers: Dordrecht, The Netherlands, 670 pp.

Weber, R.O., 1998: Estimators for the standard deviations of lateral, longitudinal, and vertical wind components. *Atmos. Environ.*, 32, 3639-3646.